Influence of processing parameters on mechanical properties of a 3D-printed trabecular bone microstructure

Morteza Amini [ORCID],[1,2] **Andreas Reisinger,**[2] **Dieter H. Pahr**[1,2]

[1]Institute for lightweight design and structural biomechanics, Vienna University of Technology, 1060 Vienna, Austria
[2]Department of Anatomy and Biomechanics, Karl Landsteiner University for Health Sciences, 3500 Krems, Austria

Abstract: Natural bone microstructure has shown to be the most efficient choice for the bone scaffold design. However, there are several process parameters involved in the generation of a microCT-based 3D-printed (3DP) bone. In this study, the effect of selected parameters on the reproducibility of mechanical properties of a 3DP trabecular bone structure is investigated. MicroCT images of a distal radial sample were used to reconstruct a 3D ROI of trabecular bone. Nine tensile tests on bulk material and 54 compression tests on 8.2 mm cubic samples were performed (9 cases × 6 specimens/case). The effect of input-image resolution, STL mesh decimation, boundary condition, support material, and repetition parameters on the weight, elastic modulus, and strength were studied. The elastic modulus and the strength of the bulk material showed consistent results (CV% = 9 and 6%, respectively). The weight, elastic modulus, and strength of the cubic samples showed small intragroup variation (average CV% = 1.2, 9, and 5.5%, respectively). All studied parameters had a significant effect on the outcome variables with less effect on the weight. Utmost care to every step of the 3DP process and involved parameters is required to be able to reach the desired mechanical properties in the final printed specimen. © 2019 The Authors. *journal Of Biomedical Materials Research Part B: Applied Biomaterials* Published By Wiley Periodicals, Inc. J Biomed Mater Res Part B: Appl Biomater 108B:38–47, 2020.

Key Words: 3D printing, scaffolds, tissue engineering, process parameters, trabecular microstructure

INTRODUCTION

Since its development more than 30 years ago, the 3D printing (3DP) technology (e.g., additive manufacturing or AM) has gained tremendous attraction in the field of medicine and biomedical sciences during the past few years.[1,2] In the field of tissue engineering, the possibility of producing sophisticated porous structures with a fraction of the cost compared to typical manufacturing methods has made 3DP the preferred option for scaffold production. Specifically, microscale scaffolds for bone replacement and regeneration are of great interest.[1,3–12]

Bone scaffolds temporarily replace the defected or lost bone section until the regeneration process is taken place and new bone tissue is produced. The mechanical properties (stiffness and strength) of scaffolds used for bone regeneration play an important role in determining the possibility and quality of cell regrowth and proliferation.[4,13,14] These properties are governed by the geometry of the structure and the tissue/printing material properties. A scaffold much stiffer or much softer than the surrounding bone tissue would result in osteopenia or fracture.[15]

A typical approach to achieve a spongy structure similar to trabecular bone is to generate a repeating structural block composed of simple geometries, such as rods and spheres. This method results in a generic 3D structure for the scaffold, which can be mass produced and used for different applications and sites. However, it has been shown that such homogeneous structures with uniform porosity used for bone regeneration purposes exhibit uniform strain distribution within the structure, while a heterogeneous gradient of strain might be necessary for remodeling of osseous tissue.[16–18] It has also been previously shown that structural differences highly impact the mechanical properties of the scaffolds, emphasizing on the necessity of structural compatibility of the scaffold and its intended site.[19–22]

It is currently widely accepted that the optimum scaffold structure for bone regeneration and remodeling purposes should mimic natural bone properties at all levels including mechanical and microstructural parameters of the specific site or environment in which the scaffold will be used.[10,23–33] Therefore, a major objective of bone tissue engineering has become to achieve geometries as similar to trabecular bone as possible.[3,4,34]

Using micro-CT imaging technique, the 3D trabecular structure of the bone can be captured in microscale resolutions (typically around 10-micron voxel size). The captured

Correspondence to: M. Amini; e-mail: morteza.amini@tuwien.ac.at

image data can be processed and prepared to be used for replicating the same structure using 3DP. The path toward a printed trabecular bone sample based on CT image data involves imaging of the bone, followed by processing the image (i.e., crop and segment) to extract a surface covering the bone volume (e.g., an STL file), which, after further processing, is finally sent to the 3D printer. Each of these steps include multiple parameters, which have minor or major effects on the structure, such as image resolution, object feature size, mesh simplification (decimation), printing orientation, printing resolution, material type, printing method, support material removal, and so forth. The structural properties (geometrical and mechanical properties) of the printed sample are directly dependent on the selected parameters.

The correct reproduction of the input geometry and structure is of great importance to achieve the required structural function of the printed specimen.[1,35,36] However, high resolutions result in huge STL files, which cannot be handled by commercial 3D printers and make mesh simplification steps inevitable. Up to now the influence of such simplifications on the printed structure is not investigated.

Looking at the commercially produced scaffolds with simple structural units, and manufactured simultaneously in batches, significant difference in terms of their mechanical properties within a batch as well as between different batches are found.[13] One reason for this high sensitivity is a power-law that connects the density to the elastic and yield properties (e.g., the overall elastic modulus of a cancellous structure, such as trabecular bone, is a power-law function of the bone volume fraction).[37] This implies the importance of determining the reproducibility of mechanical properties of printed scaffolds. The unavailability of a standard detailing the process parameters for every step involved in 3DP of medical-related objects has been viewed as the main barrier for certification of AM components and methods to be used.[1] Consequently, benchmark tests to reach to a standardized methodology and process for 3DP of the medical objects are deemed necessary by multiple groups in this field.[1,4,38–40] There have been multiple studies investigating the inherent errors of different steps involved in the medical rapid prototyping methods.[1,41–57] Nevertheless, all these studies have fallen short of demonstrating the effect of such errors on the mechanical properties of printed objects and conducting a systematic search for different sources of error. In this sense, the goal of this study is to investigate the effect of selected processing parameters on the reproducibility of mechanical stiffness and strength of a 3DP trabecular bone structure. These preliminary investigations are intended to demonstrate the importance of choosing the correct value for these parameters, while being aware of the magnitude of effect that each of them will have on the stiffness, strength, and ultimately the functionality of the printed structure.

METHODS AND MATERIALS
CT scanning and image processing
MicroCT images (μCT 100, Scanco Medical, AG, Brüttisellen, Switzerland-16.4 μm, 70 kV, 200 μA, 300 s) of a cadaveric distal radius sample with 16 μm resolution were taken followed by extraction of an $8.2 \times 8.2 \times 8.2 \text{ mm}^3$ cubical ROI from the metaphysis region. The workflow is shown in Figure 1. All image processing, mesh manipulations, and print data file generations are done with medtool (www.dr-pahr.at, Austria) and using VTK libraries (www.vtk.org).

To select the ROI, the two parameters of bone volume fraction (BV/TV) and mean trabecular orientation were considered. A moving cube with the mentioned dimensions was used in a way that the cube was containing only trabecular bone. Multiple instances of the ROI were selected and for each instance the BV/TV and mean trabecular orientation (using the mean intercept method (MIL) for determining anisotropy) were calculated in medtool. The ROI with the closest BV/TV to the reported average values (16.5%)[58] and the least deviation of the mean trabecular orientation from vertical axis (7 degrees) was selected to get a representative sample, which is nearly oriented in the axes of orthotropy of the distal radius. An automatic segmentation method[72] was used to create the binary version of the ROI for further processing and STL file generation. A series of test prints were performed to specify the maximum printable complexity of the structure using the available 3D printer (OBJET EDEN 260VS™, more details are below). It was found that the largest STL file that the printer and its software package were able to process and produce was 1 GB (to put this number into perspective, the STL file of the microCT image
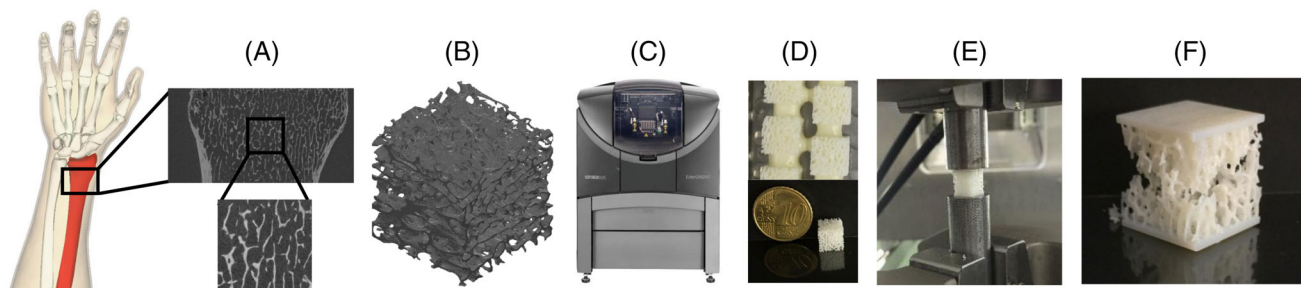
FIGURE 1. The microCT scan of a distal radius was imported into medtool software, and the ROI with most vertical axis of heterogeneity was cropped (A). The STL files were created after the specification of the desired values for the resolution, decimation, and boundary condition (B). Six samples plus a tensile test specimen were simultaneously printed for each case (C). Printed samples were postprocessed to remove the support material from the structure in an ultrasound bath (D). After weight measurement, compression tests were performed on cubic samples to determine their overall mechanical strength and stiffness (E-F).

of a 20-mm distal radial section, with no further image processing and mesh simplification steps, has around 20 GB of file size).

Printing

A Stratasys Polyjet (OBJET EDEN 260VS™) 3D printer was used to print the samples. This Polyjet printer utilizes a moving jetting head in a horizontal plane to spray fluid droplets of the photo-curing printing polymer and the support material. This results in a layer by layer deposition of the two types of material on the vertically moving tray. The printing resolution was 16 μm. The used printing material for this project was VeroWhitePlus (Tensile strength: 58 MPa, E-Modulus: 2500 MPa) with water-soluble SUP707 and normal SUP705 support materials. Despite not being a biocompatible material, the VeroWhitePlus polymer has similar mechanical properties to the Fullcure MED610 ISO 10993-1: 2009 compliant.[4] Its elastic modulus is also comparable to the PDLLA and PLGA (E = 1900 MPa) and in the same magnitude as calcium phosphate composites (E between 4000 and 11000 MPa).[59,60] Support material removal was done according to the manufacturer's instructions.[61] Samples were placed in an ultrasound bath of 1% sodium hydroxide solution throughout the removal process (up to 12 h), with ultrasound function applied for 15 min in intervals to avoid overheating, and the thermostat set at 35°C. To get optimal mechanical properties as per instructions of the manufacturer,[61] after the support material removal process was complete, the samples were dipped into a 2% glycerol solution and let dry overnight. Samples were weighed afterwards. There was a one-week gap between the printing of the samples and beginning of the support removal process, and a one-day gap between the support material removal process and the mechanical testing.

Study design

The process parameters and values chosen for this study were:

- *Resolution* of the input image used to generate the STL file. Two values of 16 and 32 μm were tested. Coarsening was done by simply grouping four neighboring pixels to form the bigger pixel twice the dimensions, and a subsequent thresholding to maintain a binary image.

- *Decimation* (AKA polygon reduction) of the surface mesh during the STL file generation. The feature angle value was used to control the decimation extent. A range of feature angle values (which determines the minimum allowable angle between two adjacent polygons) were tested to find the value with adequate geometrical details of the structure (controlled qualitatively). The 25° was the final selection (Figure 2).

- *Boundary conditions* of the samples during mechanical testing. Two different cases were tested: original/plated and free/glued. The original cubes are not constrained with any potting plate on any of the six surfaces, while the plated samples are printed with a 0.8 mm plate on the loading ends. The free cubes (regardless of being in original or plated state) are only placed on the testing machine, while the glued samples are glued to Plexiglas sheets at loading ends (with high-friction coefficient between the sheets and loading plates) (Figure 3). A thin layer of fluid instant glue was applied on the sheets with no considerable penetration into the structure.

- *Support material type* used for printing the samples. As mentioned before, two types of support material named SUP705 (normal) and SUP707 (water soluble) support materials were used.

- *Repetition* of the printing and sample preparation processes. All the steps from printing the samples until the mechanical testing were repeated for a new case and the effect of slight differences in timing of the steps involved in the whole process were observed.

Considering the printable file size limits and to investigate the effect of mentioned parameters on the mechanical properties of 3DP trabecular bone structures, nine study cases were defined (Table I). To study the reproducibility of the bulk material properties of the printing material, standard tensile test samples (ASTM D638 IV) were also designed. Six sample cubes for each study case plus a standard tensile test sample were printed stacked beside one another in each single printing job (build time between 42 and 48 min) (Figure 4). The isolated effects of parameters were extracted by comparing two cases with only one different parameter in between. STL files of each study case
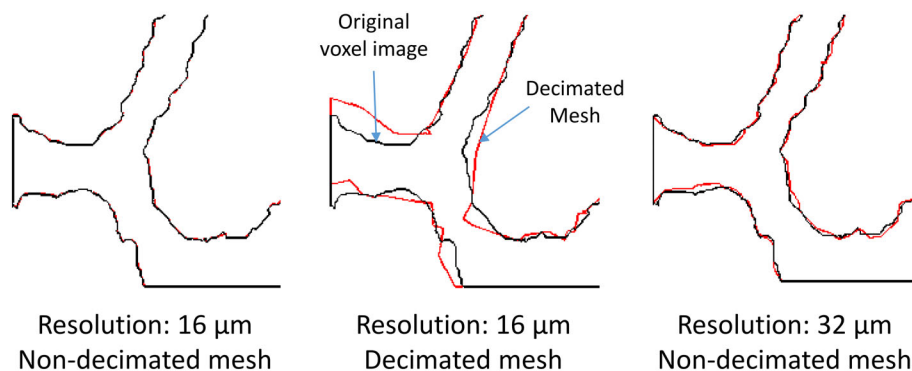
FIGURE 2. Effect of decimation and resolution on trabecular structure. The edges of the trabeculae in a planar section through the voxel image (black line) and modified surface mesh (red line) are shown.
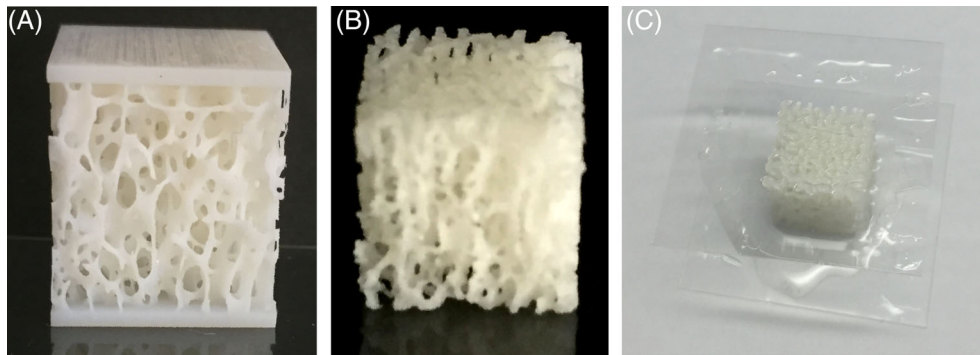
FIGURE 3. The different boundary conditions considered were (A) Free, (B) Embedded, and (C) Glued.

were produced following the workflow in Figure 1. In contrast with many commercial products in which decimation is done automatically by specifying the percentage reduction in the number of polygons, without further possibility of a user interaction, we accurately controlled this step using the "feature angle (FA)," which governs the criteria by which polygons are simplified. Sample outcomes of decimation and resolution are seen in Figure 2, with different boundary conditions shown in Figure 3.

Mechanical testing

The tensile tests on the bulk material were performed based on ASTM standard (Figure 4, bottom-left) (ASTM D638-14). Compression tests were performed on the printed bone samples using a Mini-Bionix MTS system (Figure 4, bottom-right) with 0.02 mm/s displacement controlled loading rate until 1 mm displacement was reached, which was post-failure for all specimens. The load and displacement data were recorded from the 15 kN load cell (HBM, Germany) and the cross-head of the machine to calculate the overall strength and elastic modulus of the samples.

Data evaluation

Load–displacement data from the mechanical testing machine were recorded for all tensile and cubic specimen. The structural stiffness (K) of a sample was taken from the slope of the linear section (between 40 and 60 N for the cubes) of the load–displacement plot (Figure 5). The apparent elastic modulus (E) was calculated based on the stiffness and geometrical

measurements of the sample. The apparent strength of each sample was calculated based on the ultimate load (highest recorded value on the plot, Fu) and the cross-sectional area of the specimen (A). For tensile specimen, the relative standard deviation (e.g., Coefficient of Variation or CV%) was used to show the variation of the outcome parameters among all nine samples. Also for the cube specimen, the CV% was used to report the intragroup and intergroup variation for the study cases. The intragroup variation represents the difference in the outcome variables of the six samples within a case, which is related to sources other than the altered parameter such as build time, manufacturing and testing time gap, random printing defects, and so forth. The intergroup variation is due to the effect of the altered parameter between the two cases compared to each other. The average values for weight, strength, and E-modulus of the cube samples in each case are plotted as well. Unpaired two-tailed student's t test was used to determine if the observed differences between the cases are significant (Microsoft Excel). The significance was set to $p < 0.05$.

RESULTS
Intragroup variation

The standard tensile testing of the ASTM-compliant samples printed with each study case showed consistent results in terms of weight, stiffness (E-modulus), and tensile strength (CV% = 1, 9, and 6%, respectively). The average intragroup variation of the weight, E-modulus, and overall structural strength of the cubes were 1.2, 9, and 5.5%, respectively

TABLE I. Investigated Study Cases: Nine cases are Investigated Using n = 6 Samples per Case. The Parameters Studied Using These Cases are the Input Image Resolution (16 and 32 μm), the Surface Mesh Decimation, the Boundary Conditions During Mechanical Testing, Support Material Remnant, and Repetition (C9 is the repetition of C3)

Case	Resolution (mm)	Decimation	Boundary Conditions	Water Soluble Support Material	Support Material Removal
C1	0.016	Yes	Original-free	Yes	Yes
C2	0.016	Yes	Original-glued	Yes	Yes
C3	0.016	Yes	Plated-free	Yes	Yes
C4	0.016	Yes	Plated-free	No	No
C5	0.016	Yes	Original-glued	No	No
C6	0.032	Yes	Plated-free	Yes	No
C7	0.032	NO	Plated-free	Yes	Yes
C8	0.016	NO	Plated-free	Yes	Yes
C9	0.016	Yes	Plated-free	Yes	Yes
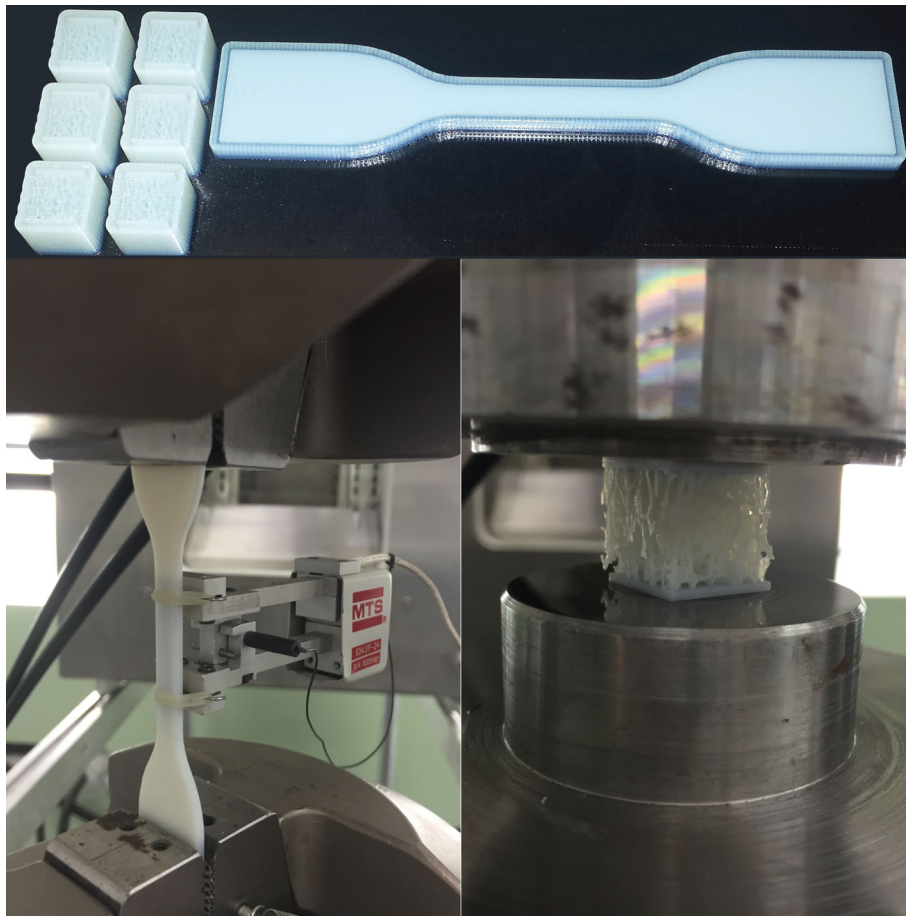
FIGURE 4. An ASTM-compliant tensile test specimen was printed with each test case (top) and was tested to determine the bulk material properties and its reproducibility (bottom-left). Trabecular bone cubes were subjected to compression between two parallel flat surfaces (bottom-right).
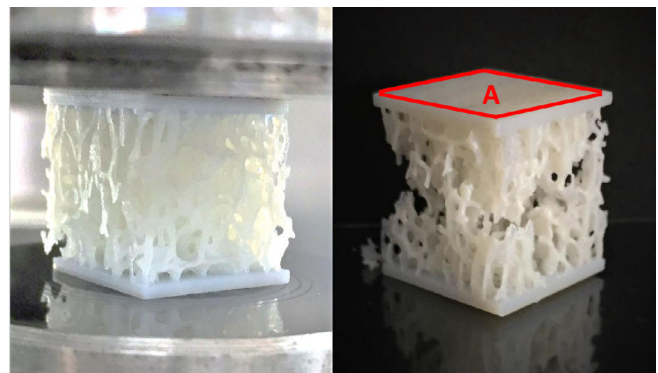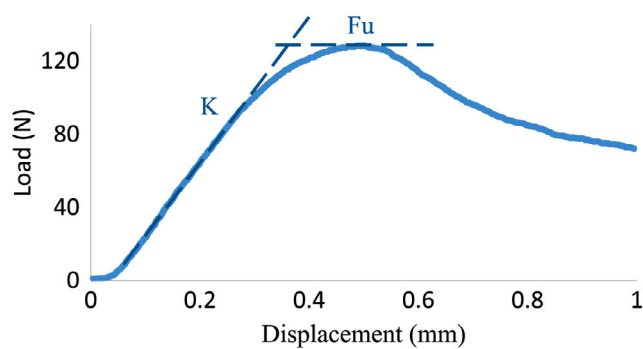
FIGURE 5. A sample load–displacement plot for a C3 specimen is shown beside the pictures of the failed specimen under loading. The elastic modulus was computed based on the stiffness taken from the slope of the linear section of the curve. The ultimate load was taken as the highest recorded load. The strength (MPa) was calculated using the ultimate load and the measured cross-sectional area of the specimen.

(range: weight 0.0–2.0%, stiffness: 3.6–12.9%, and strength 2.0–10.9%) (Table II).

Intergroup variations

To identify the effect of each selected process parameter on the outcome variables, the average value of each variable for the six samples within each case is computed (Figures 6–8). To test if the observed difference between the reported average values of two corresponding cases is significant, unpaired two-tailed student's t tests were performed. Significance was assumed for values of $p < 0.05$. The error bar of one standard deviation is included in each plot as a representation of the intragroup variation. Since the support material was not removed for cases C4, C5, and C6, they are not included in the weight outcome variable plot (Figure 6).

TABLE II. Intragroup Variation of the Outcome Parameters in terms of Coefficient of Variation (CV%). The Weight of C4-6 Samples was not Considered Because the Support Material was not Removed from These Samples

Case	Weight	E-Modulus	Strength
C1	2.0	3.6	4.2
C2	2.0	12.8	10.9
C3	1.8	10.4	2.0
C4	N/A	11.2	2.4
C5	N/A	2.8	1.6
C6	N/A	11.1	5.9
C7	0.0	4.0	4.1
C8	1.7	10.6	7.6
C9	0.0	13.0	4.1
Avg.	1.25	8.6	4.3

DISCUSSION

The aim of this study was to investigate the effects of different processing parameters on the mechanical properties of a 3DP trabecular bone structure. The selected parameters were mesh decimation, image resolution, boundary condition, support material, and repetition. The bulk material properties showed small variations for all printed samples based on the standard ASTM tensile tests. The observed variations for tensile samples were also very similar to the average intragroup variations for the trabecular cubes, meaning that the sources of these variations affected the fine structure of the cubes the same as the rough structure of the tensile samples. This enabled us to detect isolated effects of each selected process parameters on the outcome variables among the study cases.

While there has been numerous number of studies on comparing different build parameters (e.g., layer thickness, build orientation, and laser power), printing materials, structural designs, and printing technologies in terms of the geometrical and mechanical properties of scaffolds,[62–65] very few have studied reproducibility of such properties using the same processes,[13,66–69] and to our knowledge, none have yet tried to understand the effect of altering the process parameters on the mechanical properties of printed trabecular-like microstructures.

Reproducibility

Based on our results, keeping the structural parameters (density and microstructure) unchanged, and repeating the
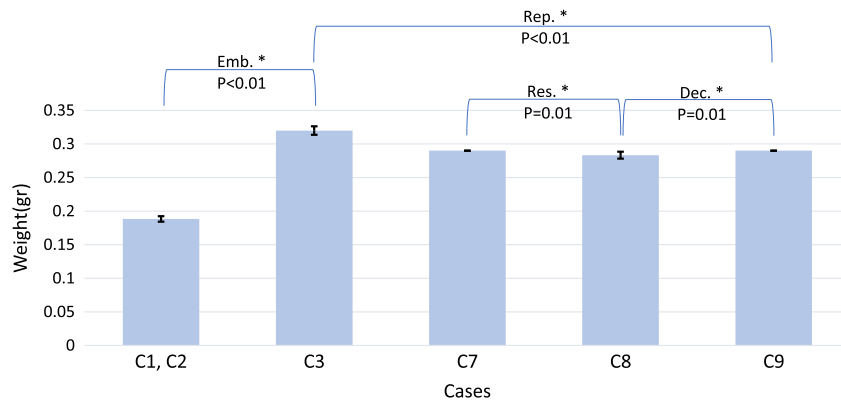
FIGURE 6. Influence of resolution (Res.), decimation (Dec.), boundary condition (embedding: Emb.), and repetition (Rep.) on weight of the samples. The average weight of the six samples in each case with one standard deviation bars. The weight of the samples for C2 and C1 are the same as they were printed and processed together. All tested parameters affected the weight of the samples significantly.
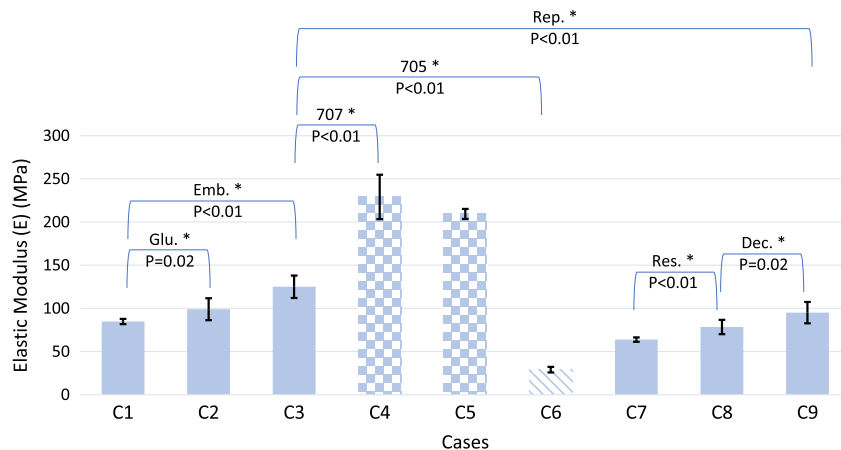
FIGURE 7. Influence of resolution (Res.), decimation (Dec.), boundary condition (glue: Glu., embedding: Emb.), repetition (Rep.), and support material remnants (normal support material: 705, soluble support material: 707) on apparent elastic modulus of the samples. Patterned bars are representing the cases with support material not removed from the samples. All tested parameters affected the elastic modulus of the samples significantly.
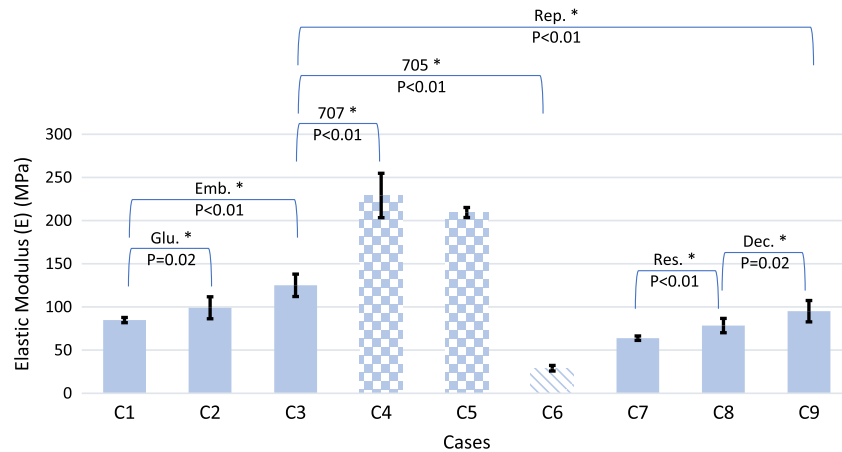
FIGURE 8. Influence of resolution (Res.), decimation (Dec.), boundary condition (glue: Glu., embedding: Emb.), repetition (Rep.), and support material remnants (normal support material: 705, soluble support material: 707) on apparent strength of the samples. Patterned bars are representing the cases with support material not removed from the samples. All tested parameters affected the strength of the samples significantly except for the glue boundary condition case.

printing, support material removal, sample preparation, and mechanical testing steps resulted in a 10, 20, and 24% difference in the weight, strength, and stiffness of the samples, respectively.

This is in line with the findings reported regarding the significant variability of the mechanical properties of different samples from a specific bone scaffold ordered from the same producer at different times.[13] Based on our observations, the time gaps between completion of the printing job, removal of the support material, and mechanical testing, the water solution temperature, the saturation level at which the water bath is refreshed, and as a result the amount of residual support material within the sample considerably affect the mechanical properties of the samples. While trying to repeat all the steps in a similar fashion, there were differences in the magnitude of minutes during the support removal process, and also hours in the interval between the end of printing process and start of the support material removal. Based on our observations, even by using automatic support removal cabinets and trying to minimize the variation in the timing of different processes, replicating mechanically identical samples might not be possible.

Support material

Our results suggest that normal (SUP705) and soluble (SUP707) support materials have reverse effect on the mechanical properties of the samples, if left on them for an extended period of time (~2 weeks). This is due to a chemical interaction between the support material and the polymer.[61] The normal support material degrades the polymer leading to a reduction in the overall strength and stiffness. However, the soluble support material hardens overtime and acts as a block of hard material with higher strength and stiffness compared to the printed structure without support material.

Glycerol coating

As an additional test, the effect of suggested glycerol coating of the printed specimens on outcome variables was tested. Repeating the complete process for selected study cases resulted in a 20, 40, and 27% difference in the average weight, strength, and stiffness of the samples (results not shown), respectively. The increased weight is due to the glycerol covering the samples gone through the support material removal steps described in the methods section. The effect of support material removal delay and glycerol coating were negligible for tensile test samples, which indicates the importance of controlling these parameters only for structures with very fine structural features. A more precise protocol with specific time intervals for each step might reduce this effect and result in less variability.

Decimation

The mesh decimation increased the strength and overall stiffness of the samples by 21 and 18%, respectively. We speculate that elimination of sharp notches and overall smoother trabecular surface may explain this effect. Cutting the resolution of the input microCT image in half resulted in a 12% increase in strength and a 22% reduction in stiffness of the samples. This inverse effect on these variables might be the result of microstructural alteration in terms of trabecular connectivity. Lower resolution results in elimination of thin connections between trabeculae but at the same time increases the trabecular thickness in other regions due to the partial volume effect. This way the overall change in weight of the sample (BV/TV) is very small (2.4% difference) (Figure 2).

Embedding

The presence of embedding in form of printed or glued plates only affected the stiffness of the samples by increasing it 32 and 20%, respectively. Based on our observations on the samples after the mechanical tests, in the samples with free-contact surfaces, the trabeculae at these areas were crushed, while the embedding prevented such damages to occur in other study groups. The difference between the printed and glued embedding is also due to the different thickness of the embedding and hence better preservation of

the contact surface trabeculae in the samples with printed embedding (Figure 3).

Mechanical properties

The decimation, resolution, and boundary condition parameters affected the mechanical properties (stiffness and strength) of the samples significantly, while having less effect on the weight of them (Figures 7–8). The average percentage difference between the E-modulus and strength of the corresponding study cases (e.g.,comparing C7 and C8 for resolution parameter) was 23 and 12%, respectively, compared to 4% for the weight outcome variable (excluding the support material cases C4, C5, and C6, because the presence of the support material visually alters the specimen, making these cases irrelevant for the intended comparison). Given the similar volume of the cubes, their similar weight means that the "bone volume fraction (BV/TV)" of the samples is not noticeably affected by the altered parameters. This results in similar-looking samples with significantly different mechanical properties, which, once more, highlights the sensitivity of the choices that should be made along the process of manufacturing 3D replications of bone tissue.

The presented study could be improved in a number of areas. First, in this study only one 3DP technology and one choice of printing polymer was used. The PolyJet AM technology has been FDA approved for bio printing[70] and in some cases has shown some superior results comparing to other typical printing technologies.[40,71] Also, the significant differences between the intragroup and intergroup variations in mechanical outcome variables eliminate the dependency of the results on the selected AM technology to some extent. However, to have a more global view over the exact effect of process parameters on mechanical properties of printed microstructures, this approach can be repeated with various printers and printing materials. Use of biocompatible/biodegradable materials should be considered to be most clinically relevant. If replication of mechanical properties of bone was intended, calcium-based printing material with bone-like properties should be tested. Second, the degree of complexity and delicacy of the printed microstructure made it extremely difficult to remove all the support material filling tiny pores of the sample. It was tested via cutting some of the samples open that even after 12 hrs of support material removal process, the core of the cubes contains some remainder of that material. The tests done on the samples with support material on them indicated the inevitable interaction between the support and printing material. To make sure that no support material remains inside the samples, scaled samples or a different removal process could be useful but is out of the scope of this study. Third, only a single cubic ROI was used to test the parameters on the printed specimens. Specimens based on ROIs from different sites and with different bone volume fraction may affect the results. Fourth, a simple uniaxial compression test was performed in this study, where the loading axis was coincident with the printing direction. However, due to the layered nature of the printed specimens off-axis loading might alter the outcomes. Finally, to study the microstructure of the printed samples after the support material removal and sample preparation, micro CT evaluation was considered and done on selected samples. However, due to the similarity of the attenuation coefficients of the printing material, support material, and the glycerol layer, we were unable to segment the printed polymer structure from the surrounding material. This also meant that no direct comparison between the BV/TV of printed samples and the input ROI was possible. Different choice of the materials might overcome this issue.

CONCLUSION

As it is mentioned in the literature that "the art of tissue engineering is where to put holes...",[24] and considering the consensus on the "efficiency" of the trabecular bone structure and geometry based on the imposed loading and boundary conditions according to mechanobiology principles, it only makes sense to strongly consider the use of natural bone-like structures in scaffolds for bone remodeling purposes. It was previously shown that the architecture of the scaffolds determines the mechanical properties of the scaffold as well as the quality and extent of cellular diffusion and growth within the structure.[20,22] As a result, various mechanical goals are being set by tissue engineers for specific scaffolds to be met through structural and geometrical manipulations and designs and using different materials. This further highlights the importance of clearly understanding the effects of different process parameters on the "optimized mechanical properties". This work has clearly shown the importance of different options of such process parameters. Informed choices, careful planning, and controlling of different steps and detailed reporting of the used parameters will help the community to be able to reproduce the desired results.

ACKNOWLEDGMENT

REFERENCES

1. Singh S, Ramakrishna S. Biomedical applications of additive manufacturing: Present and future. Current Opinion Biomed Eng 2017;2:105–115.
2. Lunsford C, Grindle G, Salatin B, Dicianno BE. Innovations with 3-dimensional printing in physical medicine and rehabilitation: A review of the literature. PM&R 2016;8(12):1201–1212.
3. Podshivalov L, Gomes CM, Zocca A, Guenster J, Bar-Yoseph P, Fischer A. Design, analysis and additive manufacturing of porous structures for biocompatible micro-scale scaffolds. Procedia CIRP 2013;5:247–252.
4. Velasco MA, Lancheros Y, Garzón-Alvarado DA. Geometric and mechanical properties evaluation of scaffolds for bone tissue applications designing by a reaction-diffusion models and manufactured with a material jetting system. J Comput Des Eng 2016;3(4): 385–397.
5. Velasco MA, Narváez-Tovar CA, Garzón-Alvarado DA. Design, materials, and mechanobiology of biodegradable scaffolds for bone tissue engineering. Biomed Res Int 2015;2015:1–21.
6. Amini AR, Laurencin CT, Nukavarapu SP. Bone tissue engineering: Recent advances and challenges. Crit Rev Biomed Eng 2012;40(5): 363–408.

7. Butscher A, Bohner M, Roth C, Ernstberger A, Heuberger R, Doebelin N, Rudolf von Rohr P, Müller R. Printability of calcium phosphate powders for three-dimensional printing of tissue engineering scaffolds. Acta Biomater 2012;8(1):373–385.

8. Suwanprateeb J, Sanngam R, Panyathanmaporn T. Influence of raw powder preparation routes on properties of hydroxyapatite fabricated by 3D printing technique. Mater Sci Eng C 2010;30(4):610–617.

9. Shanjani Y, Croos D, Amritha J, Pilliar RM, Kandel RA, Toyserkani E. Solid freeform fabrication and characterization of porous calcium polyphosphate structures for tissue engineering purposes. J Biomed Mater Res B Appl Biomater 2010;93(2):510–519.

10. Leong K, Cheah C, Chua C. Solid freeform fabrication of three-dimensional scaffolds for engineering replacement tissues and organs. Biomaterials 2003;24(13):2363–2378.

11. Gómez S, Vlad M, López J, Fernández E. Design and properties of 3D scaffolds for bone tissue engineering. Acta Biomater 2016;42:341–350.

12. Bibb R, Thompson D, Winder J. Computed tomography characterisation of additive manufacturing materials. Med Eng Phys 2011;33(5):590–596.

13. Brunelli M, Perrault C, Lacroix D. Mechanical response of 3D insert® PCL to compression. J Mech Behav Biomed Mater 2017;65:478–489.

14. Ikada Y. Challenges in tissue engineering. J Royal Soc Interface 2006;3(10):589–601.

15. Burg KJ, Porter S, Kellam JF. Biomaterial developments for bone tissue engineering. Biomaterials 2000;21(23):2347–2359.

16. Adachi T, Aonuma Y, Ito S-i, Tanaka M, Hojo M, Takano-Yamamoto T, et al. Osteocyte calcium signaling response to bone matrix deformation. J Biomech 2009;42(15):2507–2512.

17. Khoda A, Ozbolat IT, Koc B. Designing heterogeneous porous tissue scaffolds for additive manufacturing processes. Comput-Aid Des 2013;45(12):1507–1523.

18. Mullender M, El Haj A, Yang Y, Van Duin M, Burger E, Klein-Nulend J. Mechanotransduction of bone cellsin vitro: Mechanobiology of bone tissue. Med Biolog Eng Comput 2004;42(1):14–21.

19. Hutmacher DW, Schantz T, Zein I, Ng KW, Teoh SH, Tan KC. Mechanical properties and cell cultural response of polycaprolactone scaffolds designed and fabricated via fused deposition modeling. J Biomed Mater Res Part A. 2001;55(2):203–216.

20. Sobral JM, Caridade SG, Sousa RA, Mano JF, Reis RL. Three-dimensional plotted scaffolds with controlled pore size gradients: Effect of scaffold geometry on mechanical performance and cell seeding efficiency. Acta Biomater 2011;7(3):1009–1018.

21. Yeo A, Rai B, Sju E, Cheong J, Teoh S. The degradation profile of novel, bioresorbable PCL–TCP scaffolds: An in vitro and in vivo study. J Biomed Mater Res A 2008;84(1):208–218.

22. Yilgor P, Sousa RA, Reis RL, Hasirci N, Hasirci V. 3D plotted PCL scaffolds for stem cell based bone tissue engineering. Macromolecular symposia 2008;269:92–99.

23. Bose S, Roy M, Bandyopadhyay A. Recent advances in bone tissue engineering scaffolds. Trends Biotechnol 2012;30(10):546–554.

24. Hollister SJ. Porous scaffold design for tissue engineering. Nat Mater 2006;5(7):590.

25. Hutmacher DW. Scaffolds in tissue engineering bone and cartilage. Biomaterials 2000;21(24):2529–2543.

26. Hutmacher DW, Schantz JT, Lam CXF, Tan KC, Lim TC. State of the art and future directions of scaffold-based bone engineering from a biomaterials perspective. J Tissue Eng Regen Med 2007;1(4):245–260.

27. Karageorgiou V, Kaplan D. Porosity of 3D biomaterial scaffolds and osteogenesis. Biomaterials 2005;26(27):5474–5491.

28. Khan Y, Yaszemski MJ, Mikos AG, Laurencin CT. Tissue engineering of bone: Material and matrix considerations. JBJS 2008;90(Supplement_1):36–42.

29. Lichte P, Pape H, Pufe T, Kobbe P, Fischer H. Scaffolds for bone healing: Concepts, materials and evidence. Injury 2011;42(6):569–573.

30. Liu X, Ma PX. Polymeric scaffolds for bone tissue engineering. Polymeric Scaffolds for Bone Tissue Engineering. Ann Biomed Eng 2004;32(3):477–486.

31. Mathieu LM, Mueller TL, Bourban P-E, Pioletti DP, Müller R, J-AE M. Architecture and properties of anisotropic polymer composite scaffolds for bone tissue engineering. Biomaterials 2006;27(6):905–916.

32. Rezwan K, Chen Q, Blaker J, Boccaccini AR. Biodegradable and bioactive porous polymer/inorganic composite scaffolds for bone tissue engineering. Biomaterials 2006;27(18):3413–3431.

33. Willie BM, Petersen A, Schmidt-Bleek K, Cipitria A, Mehta M, Strube P, Lienau J, Wildemann B, Fratzl P, Duda G. Designing biomimetic scaffolds for bone regeneration: Why aim for a copy of mature tissue properties if nature uses a different approach? Soft Matter 2010;6(20):4976–4987.

34. Bashoor-Zadeh M, Baroud G, Bohner M. Geometric analysis of porous bone substitutes using micro-computed tomography and fuzzy distance transform. Acta Biomater 2010;6(3):864–875.

35. Niemczewska-Wójcik M, Krawczyk M, Wójcik A. The evaluation of dimensional and shape accuracy of friction pair elements: Ball-cup. XXI IMEKO World Congress, Prague, Czech Republic; 2015.

36. Zarb G, Schmitt A. The longitudinal clinical effectiveness of osseointegrated dental implants: The Toronto study. Part III: Problems and complications encountered. J Prosthet Dent 1990;64(2):185–194.

37. Currey JD. The relationship between the stiffness and the mineral content of bone. J Biomech 1969;2(4):477–480.

38. Hinton T, Lee A, Feinberg AW. 3D bioprinting from the micrometer to millimeter length scales: Size does matter. Current Opinion Biomed Eng 2017;1:31–37.

39. Kim G, Oh Y. A benchmark study on rapid prototyping processes and machines: Quantitative comparisons of mechanical properties, accuracy, roughness, speed, and material cost. Proc. Institut. Mech. Eng., Part B: J. Eng. Manufac. 2008;222(2):201–215.

40. Salmi M, Paloheimo K-S, Tuomi J, Wolff J, Mäkitie A. Accuracy of medical models made by additive manufacturing (rapid manufacturing). J Craniomaxillofac Surg 2013;41(7):603–609.

41. Arrieta C, Uribe S, Ramos-Grez J, Vargas AP, Irarrazaval P, Parot V, et al. Quantitative assessments of geometric errors for rapid prototyping in medical applications. Rapid Prototyping Journal 2012;18(6):431–442.

42. Bibb R, Winder J. A review of the issues surrounding three-dimensional computed tomography for medical modelling using rapid prototyping techniques. Radiography 2010;16(1):78–83.

43. Choi JY, HJ Choi , Kim N, Kim Y, Lee J-K, Kim MK, et al. Analysis of errors in medical rapid prototyping models 2002. 23–32 p.

44. Ciocca L, De Crescenzio F, Fantini M, Scotti R. CAD/CAM and rapid prototyped scaffold construction for bone regenerative medicine and surgical transfer of virtual planning: A pilot study. Comput Med Imaging Graph 2009;33(1):58–62.

45. El-Katatny I, Masood S, Morsi Y. Error analysis of FDM fabricated medical replicas. Rapid Prototyping Journal 2010;16(1):36–43.

46. Galeta T, Kljajin M, Karakašić M. Geometric Accuracy by 2-D Printing Model. Journal of Mechanical Engineering 2008;10(54):725–733.

47. Germani M, Raffaeli R, Mazzoli A. A method for performance evalution of RE/RP systems in dentistry. Rapid Prototyping Journal 2010;16(5):345–355.

48. Knox K, W Kerber C, Singel S, J Bailey M, G Imbesi S. Stereolithographic vascular replicas from CT scans: Choosing treatment strategies, teaching, and research from live patient scan data. American Journal of Neuroradiology 2005;26(6):1428–1431.

49. Meakin J, E T Shepherd D, Hukins D. Fused deposition models from CT scans. Br J Radiol 2004;77(918):504–507.

50. Nizam A, N. Gopal R, Naing L, B. Hakim A, Samsudin A. Dimensional accuracy of the skull models produced by rapid prototyping technology using stereolithography apparatus. Archives of Orofacial Sciences 2006;1:60–66.

51. Pinto JM, Arrieta C, Andia ME, Uribe S, Ramos-Grez J, Vargas A, Irarrazaval P, Tejos C. Sensitivity analysis of geometric errors in additive manufacturing medical models. Med Eng Phys 2015;37(3):328–334.

52. Russett S, Major P, Carey J, Toogood R, Boulanger P. An experimental method for stereolithic mandible fabrication and image preparation. The Open Biomedical Engineering Journal 2007;1(1):4–10.

53. Sarment D, Sukovic P, Clinthorne N. Accuracy of implant placement with stereolithographic surgical guide. Int J Oral Maxillofac Implants 2003;18(4):571–577.

54. Schicho K, Figl M, Seemann R, Ewers R, Lambrecht T, Wagner A, et al. Accuracy of treatment planning based on stereolithography in computer assisted surgery. Med Phys 2006;33(9):3408–3417.

55. Silva D, Gerhardt De Oliveira M, Meurer E, Meurer M, Silva J, santa barbara A. Dimensional error in selective laser sintering and 3D-printing of models for craniomaxillary anatomy reconstruction. J Craniomaxillofac Surg 2008;36(8):443–449.

56. Wang C-S, A. Wang W-H, Lin M-C. STL rapid prototyping bio-CAD model for CT medical image segmentation. Computers in Industry 2010;61(3):187–197.

57. Winder J, Bibb R. Medical rapid prototyping technologies: State of the art and current limitations for application in oral and maxillofacial surgery. J Oral Maxillofac Surg 2005;63(7):1006–1015.

58. Khosla S, Riggs L, Atkinson E, Oberg A, McDaniel L, Holets M, Peterson J, Melton J. Effects of sex and age on bone microstructure at the Ultradistal radius: A population-based noninvasive in vivo assessment. J Bone Mineral Res 2006;21(1):124–131.

59. Chen Q, Zhu C, Thouas GA. Progress and challenges in biomaterials used for bone tissue engineering: Bioactive glasses and elastomeric composites. Prog Biomater 2012;1:2.

60. Wahl D, Czernuszka J. Collagen-hydroxyapatite composites for hard tissue repair. Eur Cell Mater 2006;11:43–56.

61. Stratasys. User guide: Object Eden 260VS 3D printer system; 2014

62. Butscher A, Bohner M, Hofmann S, Gauckler L, Müller R. Structural and material approaches to bone tissue engineering in powder-based three-dimensional printing. Acta Biomater 2011;7(3):907–920.

63. Caulfield B, McHugh P, Lohfeld S. Dependence of mechanical properties of polyamide components on build parameters in the SLS process. J Mater Process Technol 2007;182(1):477–488.

64. Farzadi A, Solati-Hashjin M, Asadi-Eydivand M, Osman NAA. Effect of layer thickness and printing orientation on mechanical properties and dimensional accuracy of 3D printed porous samples for bone tissue engineering. PloS One 2014;9(9):e108252.

65. Li M, Tian X, Chen X. A brief review of dispensing-based rapid prototyping techniques in tissue scaffold fabrication: Role of modeling on scaffold properties prediction. Biofabrication 2009;1(3):032001.

66. Castilho M, Dias M, Gbureck U, Groll J, Fernandes P, Pires I, Gouveia B, Rodrigues J, Vorndran E. Fabrication of computationally designed scaffolds by low temperature 3D printing. Biofabrication 2013;5(3):035012.

67. Chua C, Liu M, Chou S, editors. Additive manufacturing-assisted scaffold-based tissue engineering. Innovative Developments in Virtual and Physical Prototyping, Proceedings of the 5th International Conference on Advanced Research in Virtual and Rapid Prototyping, Leiria, Portugal; 2011.

68. Gbureck U, Hölzel T, Klammert U, Würzler K, Müller FA, Barralet JE. Resorbable dicalcium phosphate bone substitutes prepared by 3D powder printing. Adv Funct Mater 2007;17(18):3940–3945.

69. Serra T, Planell JA, Navarro M. High-resolution PLA-based composite scaffolds via 3-D printing technology. Acta Biomater 2013;9(3):5521–5530.

70. Yu AW, Khan M. On-demand three-dimensional printing of surgical supplies in conflict zones. J Trauma Acute Care Surg 2015;78(1):201–203.

71. Ibrahim D, Broilo TL, Heitz C, de Oliveira MG, de Oliveira HW, Nobre SMW, dos Santos Filho JHG, Silva DN. Dimensional error of selective laser sintering, three-dimensional printing and PolyJet™ models in the reproduction of mandibular anatomy. J Craniomaxillofac Surg 2009;37(3):167–173.

72. Ridler T, Calvard S. Picture Thresholding using an iterative selection method. IEEE T Syst Man Cyb 1978;8:630–632.